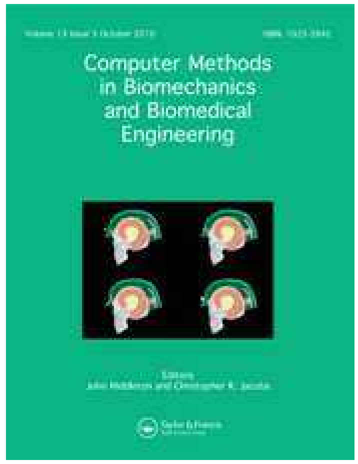

Sensitivity analysis of permeability parameters of bovine nucleus pulposus obtained through inverse fitting of the nonlinear biphasic equation: effect of sampling strategy

Journal:	*Computer Methods in Biomechanics and Biomedical Engineering*
Manuscript ID:	GCMB-2010-0235.R1
Manuscript Type:	Special Issue Paper
Date Submitted by the Author:	26-Nov-2010
Complete List of Authors:	Riches, Philip; University of Strathclyde, Bioengineering Unit
Keywords:	intervertebral disc, articular cartilage, poroelasticity

Sensitivity analysis of permeability parameters of bovine nucleus pulposus obtained through inverse fitting of the nonlinear biphasic equation: effect of sampling strategy

Philip E. Riches

Bioengineering Unit, University of Strathclyde, Glasgow, United Kingdom.

Dr P.E. Riches
Bioengineering Unit
Wolfson Building
106 Rottenrow
Glasgow
G4 0NW
United Kingdom

Tel: +44 141 548 5703
Fax: +44 141 552 6098
Email: philip.riches@strath.ac.uk

Sensitivity analysis of permeability parameters of bovine nucleus pulposus obtained through inverse fitting of the nonlinear biphasic equation: effect of sampling strategy

Permeability controls the fluid flow into and out of soft tissue, and plays an important role in maintaining the health status of such tissue. Accurate determination of the parameters that define permeability is important for the interpretation of models that incorporate such processes. This paper describes the determination of strain-dependent permeability parameters from the nonlinear biphasic equation from experimental data of different sampling frequencies using the Nelder-Mead simplex method. The ability of this method to determine the global optimum was assessed by constructing the whole manifold arising from possible parameter combinations. Many parameter combinations yielded similar fits, with the Nelder-Mead algorithm able to identify the global maximum to within the resolution of the manifold. Furthermore, the sampling strategy affected the optimum values of the permeability parameters. Therefore, permeability parameter estimations arising from inverse methods should be utilised with the knowledge that they come with large confidence intervals.

Keywords: intervertebral disc; articular cartilage; poroelastic

Acknowledgements: The author would like to thank (name to be inserted) for their skill and patience in collecting the experimental data presented in this paper.

Introduction

Constitutive equations that describe the mechanical behaviour of cartilaginous tissue, such as the intervertebral disc, are often parameterised by fitting a biphasic, or poroelastic, model to experimental confined compression data. Such inverse techniques extract stiffness and permeability values in a given direction, which are necessary for implementation in larger scale multi-dimensional mathematical models. Such finite element models, for example of a spinal motion segment, typically assess the nutritional and mechanical functioning of the tissues (e.g. Ferguson et al., 2005) which then give rise to theories as to the mechanical aetiology of tissue degeneration. Given that fluid flow, which dictates the time dependent processes in such tissue, is principally governed by the tissue's permeability, accurately characterising tissue permeability is a necessity for the correct analysis and interpretation of these large models.

However, whenever an inverse technique is used to determine a tissue's parameters, questions arise concerning the topography of the manifold, defined by the parameter-space, which describes the goodness of fit of the model to the experimental data. Two key questions are: (1) does the manifold contain a clearly defined global optimum or do many parameter combinations yield similar fits, and (2) how smooth is the manifold: do local maxima exist as a result of surface roughness or functional variation that could affect a optimising strategy finding the global maximum? A understanding of this manifold is therefore an important aspect of utilising an inverse technique.

The biphasic theory that is able to describe the deformation of soft tissue was derived in its current form by Mow et al. (Mow et al., 1980) but is ultimately of a similar form to poroelastic theory originally developed much earlier (Biot, 1947, 1956). This linear form, where strains are assumed infinitesimal and Hookean, and permeability is independent of strain, has been extended to finite deformations (Holmes, 1986). In the finite deformation model, nonlinear constitutive equations relating the matrix stress and permeability with strain can be implemented, resulting in better numerical fits to experimental data (Périé et al., 2005). In 1997, Ateshian et al. used this finite deformation model to characterise articular cartilage, noting that the model was rather insensitive to one permeability parameter in particular. With regards to spinal tissues, a few sensitivity analyses have been made which assess the effect of varying material parameters on the larger models of spinal motion (Jones and Wilcox, 2008). Most have concentrated on the Young's moduli of the various components of the spine (Guo et al., 2009; Rao and Dumas, 1991); whilst Martinez et al. (1997) and more recently Malandrino et al. (2009) have highlighted the importance and sensitivity of permeability to the poromechanical functioning of the disc.

Despite the importance of permeability in the mechanical functioning of the being known for some time, the effect of the experimental methodologies and inverse techniques adopted to identify these material parameters has not been examined. For example, the methodology adopted to extract the material parameters is rarely presented (Ateshian et al., 1997; Johanessen et al, 2005; Périé et al., 2005) and this may have considerable effect on the parameters obtained. Secondly, it has been recently shown that the sampling methodology may have an effect on the material parameters obtained from such inverse methods (Riches, 2010). This latter work alludes to the question whether there is an optimum sampling methodology for the determination of such parameters?

This paper aims to clarify the sensitivity of the nonlinear biphasic model to sampling strategies and to changes in the permeability parameters of bovine nucleus pulposus by specifically investigating the extent of the manifold of the permeability parameter space which describes the fit to experimental data. Furthermore, the ability of a common optimising technique, the Nelder-Mead simplex method, to identify the global maximum of the goodness of fit criterion and the number of local maxima of the goodness of fit criterion are also investigated.

Methods

Experimental Methods

Motion segments from bovine tails (aged 14–30 months) were isolated, and the three discs adjacent to the tail base were dissected using a scalpel. Discs were frozen at -20 °C within 9 hours of slaughter. From the frozen specimens, axially oriented plugs of NP tissue, diameter 10mm, were obtained using a cork borer, and plugs were further microtomed to cylindrical specimens to approximately 1mm in height at -14 °C. Eight samples were obtained via this protocol and were tested in 0.15M NaCl in confined compression in a custom built apparatus (Heneghan and Riches, 2008a). The apparatus contained an impermeable acrylic confining chamber, with upper and lower compression platens made from rigid, porous, sintered 316L stainless steel (average pore size: 100 μm). The permeability of the porous platens was four orders of magnitude greater than tissue permeability, causing negligible additional resistance to flow. The upper platen was connected to the 1kN load cell (KAP-S, Angewandte System Technik AST, Wolnzach, Germany) of a materials testing machine (Model Z005, Zwick Roell, Ulm, Germany).

Each frozen sample was placed in the chamber and the porous platen was lowered until a force reading of 0.3N was achieved and the sample thickness was found from the platen-to-platen separation (1.14 ± 0.08 mm, mean ± S.D.), which was denoted the zero strain condition. The saline was added and samples thawed at room temperature and at zero strain for 2 hours to reach stress equilibrium. A ramp-hold compression was applied to 10% compressive strain (stretch ratio, $\lambda = 0.9$), with a ramp speed of 2 μm/s and a hold time of 2000s. The stress and displacement were recorded nonlinearly with a data collected every change in stress of 0.1 N, or a displacement of 0.2 μm, or an elapsed time of 5 s, and the stress–displacement relationship of the chamber was deducted from the overall displacement. All data were then resampled in Matlab (The Mathworks, Inc., U.S.) using the linear interpolation function, to linear sampling frequencies of 0.1, 0.5, and 1 Hz.

The nonlinear biphasic equation

The finite deformation biphasic model of Holmes (1986) was used in this analysis,

$$\frac{\partial U}{\partial t} = \frac{k}{\lambda}\frac{\partial \sigma_s}{\partial \lambda}\frac{\partial^2 U}{\partial Z^2} \qquad (1)$$

where U is the displacement of the tissue in the Z direction at time t, and λ is the stretch ratio ($\lambda = 1 + \frac{\partial U}{\partial Z}$). The hydraulic permeability, k, has units of m^4/Ns and is defined as the permeability of the matrix divided by the viscosity of the fluid. In this case, the viscosity of aqueous 0.15M NaCl is 0.001015 Pa.s (Lide, 1991). The hydraulic permeability has been related to deformation using (Lai and Mow, 1980):

$$k = k_0 e^{M(\lambda - 1)} \qquad (2)$$

and is characterised by an initial zero-strain permeability, k_0, and a nonlinear coefficient, M, describing the loss of permeability with compression. The stress in the solid matrix, σ_s due to compression, was given as (Holmes and Mow, 1990):

$$\sigma_s = \frac{1}{2} H_{A0}\left(\frac{\lambda^2 - 1}{\lambda^{2\beta+1}}\right) e^{\beta(\lambda^2 - 1)} + \sigma_{\pi 0} \qquad (3)$$

This equation includes the initial swelling stress, $\sigma_{\pi 0}$, which can be thought of as a combination of the osmotic stress and residual stress in the solid matrix in the zero strain condition (Heneghan and Riches, 2008a).

Parameter Estimation:

For each sample, $\sigma_{\pi 0}$ was taken as the experimental stress at $t = 0$, and H_{A0} was determined from the equilibrium stress at the end of each experiment, using $\beta = 0.256$ (Heneghan and Riches, 2008a). Thus H_{A0}, β and $\sigma_{\pi,0}$ were fixed for each sample, leaving only the permeability parameters to be determined using the time-dependent data. Equations 1 to 3 were then solved using custom written code in Matlab (The Mathworks, Inc., U.S.), using finite differences. At each time step, the experimental displacement was prescribed to the model, and the stress at the surface was calculated and compared to the experimental surface stress value. A coefficient of determination was used to characterise the goodness of fit in the stress relaxation phase, where in equation 5 the dash represents the model data, and no dash represents experimental data (Riches et al., 2002; Soltz and Ateshian, 2000):

$$R^2 = 1 - \frac{\sum(\sigma_S - \sigma_S')^2}{\sum(\sigma_S - \overline{\sigma_S})^2} \tag{5}$$

To describe the permeability parameter manifold, permeability values were systematically increased from $k_0 = 1 \times 10^{-16}$ m^4/Ns to $k_0 = 2 \times 10^{-14}$ m^4/Ns in steps of 1 x 10^{-16} m^4/Ns. Within each k_0 step, M was stepped between 0 and 15 by an increment of 0.1, creating a mesh of a possible 30000 iterations, however, within each M-step, once the R^2 had reached a maximum and the decreased below zero, the M step was ended, significantly reducing the number of iterations required to be computed. A global maximum, R^2_{max}, was determined from this data and the manifold was extended in the k_0 direction if R^2 values at $k_0 = 2 \times 10^{-14}$ m^4/Ns were greater than or equal to $0.95R^2_{max}$. This extension was required for two specimens. Local maxima were determined from the final manifold if the R^2 value of a solution using parameters

$k_{0,i}$ and M_j was greater than its surrounding 8 neighbours on the manifold and if the R^2 value was greater than or equal to $0.95R^2_{max}$ (Figure 1).

In addition to the manifold mapping, a custom-written Nelder-Mead simplex scheme was used to obtain optimal values of k_0 and M which minimised 1 - R^2, always starting the simplex in the same place, with vertices in (k_0, M) space of (1 x 10^{-14}, 0), (1.25 x 10^{-14}, 1) and (1.5 x 10^{-14}, 0). The scheme iterated until it converged, which was defined by the coordinates of the three vertices and the R^2 values at each vertex differing by less than 0.1% from the vertex with the current highest R^2 value.

The above parameter estimation procedures were repeated for each sampling strategy. Optimum k_0 and M values and the resulting R^2 were assessed with respect to sampling strategy and the methodology (mapping or Nelder Mead) using a two-way repeated measures ANOVA. Furthermore, the difference in coordinates in (k_0, M) space of the maximum R^2 between the mapping methodology and the Nelder-Mead methodology, the number of local maxima in the mapping methodology and the range and area of the region containing all values that were equal to or greater than $0.95R^2_{max}$ were determined and assessed with respect to sampling strategy using an one-way repeated measures ANOVA. Statistical significance was taken at $p \leq 0.05$, and where significant differences with sampling were found, these were further probed using t-tests with Bonferroni adjustment for multiple comparisons.

Results

The nonlinear sampling strategy resulted in a distribution of sampling frequencies throughout the stress relaxation phase (Figure 2). In the first 10 seconds of relaxation, the experimental data were sampled at rates in excess of 1Hz with 10% of this epoch being sampled at > 50 Hz. In the subsequent 90 seconds, approximately half the data were sampled at rates under 1 Hz, whilst after 100s of relaxation, nearly all the data were sampled at sub 1Hz (usually 0.2 Hz). Thus the nonlinear sampling strategy focuses the data collection toward the initial moments of stress relaxation.

Figure 3 depicts the solution manifold for a typical sample together with the route the Nelder Mead scheme took over this manifold from its starting position. Contours of constant R^2 are provided at $R^2 = 0.9$, 0.95 and 0.99. The general shape of the manifold was the same for all samples. For any value of k_0 on the manifold, the goodness of fit slowly increased with increasing M up to a maximum value. Once that maximum had been reached, further increase in M dramatically reduced R^2. A ridge existed which may be described as following a logarithmic path, i.e. $M \propto \log(k_0)$, with all local and global maxima existing on this ridge.

Figures 4, 5 and 6 depict the manifold for the same sample as figure 3, but using linear sampling frequencies of 0.1, 0.5 and 1 Hz. Qualitatively, these figures suggest that as the sampling frequency increases, the range and area of k_0 and M values than contain $R^2 \geq 0.95R^2_{max}$ decreases.

Figure 7 depicts a typical sample stress history which has been fitted by the models. Figure 7a shows the whole time history through the ramp to equilibrium, whilst Figure 7b zooms in on the first two minutes of the hold phase. Over the length of the experiment, there is no discernable difference in fitting due to the sampling scheme (Figure 7a), whilst focussing in on the initial phase of the hold phase shows that fitting to the 0.1Hz sampled data does not provide an adequate response in this region.

The permeability parameters that describe the R^2_{max} for the Nelder Mead scheme and for the mapping scheme are provided in Table 1. k_0, M and R^2 varied with sampling strategy ($p < 0.05$, $p < 0.01$ and $p < 0.001$ respectively), but only R^2 varied with curve-fitting methodology ($p < 0.05$) despite Table 1 indicating otherwise. The absolute difference between the groups, however, was of the order of 10^{-5} (Table 2). Further post hoc analysis revealed no specific differences between each sampling strategy for k_0, but the nonlinear strategy created a greater M than sampling at 0.5 Hz and 1 Hz (both $p < 0.05$). The nonlinear R^2 values were significantly greater than all of the linear strategies (all $p < 0.05$), with the linear strategies being statistically equivalent to each other.

Differences in the parameters between the curve fitting schemes did not vary across the sampling strategies, however the range of k_0 ($p < 0.05$) and M ($p < 0.001$) and the number of local maxima ($p < 0.001$) all varied with sampling strategy. Post hoc analysis suggested that no differences existed between the strategies for the range of k_0, but the nonlinear sampling strategy created a larger M range ($p < 0.001$), area ($p < 0.05$) and exhibited a higher number of local maxima ($p < 0.05$) than the linear strategies, which were statistically equivalent.

Discussion

The rationale concerning using nonlinear sampling is that it would capture the most important aspects of the data shape, in the least number of data points. Indeed the adopted nonlinear sampling protocol was intended to fully capture the fast stress relaxation portion of the data, which would focus the goodness of fit algorithm in this region. The sampling frequency distribution (Figure 2) attests to this fact. It was envisaged that increasing the data collected in the time period where there is high fluid flux would make the numerical model more sensitive to the permeability parameters. However, this wasn't found to be the case as discussed later. Furthermore, the fact that sampling strategy affected the permeability parameters obtained from the Nelder-Mead algorithm and manifold is also cause for concern. Nevertheless, since permeability affects the time-dependent processes, which is in this case the stress relaxation, it is felt that nonlinear sampling which focuses the experimental data in this area should provide a more appropriate parameterisation (Riches, 2010).

The manifolds of Figures 3 to 6 highlight the fact that, irrespective of sampling strategy, many combinations of permeability parameters can yield similar goodness of fit scores. For example, for the sample shown in Figure 2 to 5, when using the nonlinear sampling strategy, a k_0 of 3.5 x 10^{-15} m^4/Ns and an M of 6.2 yield the same goodness of fit as when using k_0 = 8.3 x 10^{-15} m^4/Ns with an M of 8.8 (R^2 = 0.994 in both cases). Consequently, whilst Ateshian et al. (1997) suggested that the nonlinear biphasic equation was insensitive to M, mapping the whole manifold has indicated that it is insensitive to both k_0 and M, if they are varied appropriately. It must be noted that two samples had very high ranges of k_0, which have skewed the results somewhat. Removing these from the analysis suggests that the range of k_0 values that can results in an R^2 of 95% R^2_{max} are approximately half those presented in Table 2. However, since there is no experimental reason why these samples should be removed from the analysis, it may be presumed that their high ranges reflect an inherent issue with curve-fitting to some biological samples. Using a linear sampling strategy reduces the extent and area of the area covering 95% of R^2_{max} but whilst statistically significant, the author's opinion is that it is not dramatic: the number of possible combinations of M and k_0 that yield a good fit to the data are high no matter what sampling strategy is used. Figures 7a and 7b adds weight to this statement, with visibly good fitting overall, and it is only the model data arising from fitting to the 0.1 Hz sampling scheme which does not adhere well to the experimental data at early times in the hold phase.

What is also of concern is the number of local maxima that exist on the manifold, in particular when the nonlinear sampling strategy was used. These local maxima may prevent numerical schemes finding the global optimum set of parameters. When expressed as a percentage of the optimum parameters determined by the Nelder Mead scheme, these differences between the curve fitting schemes was approximately 2% for k_0 and 1% for M, and for most cases were within the resolution of the manifold itself. The significant difference between the R^2_{max} determined by the two curve fitting schemes demonstrated that the Nelder Mead methodology always found the highest R^2 value. The number and nature of the local maxima suggest that these are more due to a surface roughness of the manifold, possibly as a consequence of experimental variation in the applied stress, as opposed to any large functional features on the manifold. Consequently, for this data set, it can be stated that the Nelder Mead scheme was not overtly hindered by the local maxima, and that it is able to determine the global maximum for the nonlinear biphasic equation. Linear sampling strategies reduced the number of local maxima on the manifold, with a minimum number occurring using a sampling frequency of 0.5 Hz. This may suggest that the process of resampling the data into linear forms had an effect similar to low pass filtering. If the experimental data are smooth it is hypothesised that there would be fewer local maxima on the solution manifold.

One limitation of this study is that only one level of compression ($\lambda = 0.9$) was compared. Although this was the case, the model solutions demonstrate that significant localised deformations occurred up to $\lambda = 0.4$, which indicates that a wide range of permeabilities existed within each sample during testing. It may be suggested, therefore, that the parameters obtained from fitting equation 2 were determined over a considerable range of λ, and not just up to $\lambda = 0.9$. A further limitation was that only the solution manifold regarding the permeability parameters was analysed. Indeed the stiffness constants were kept as constant as possible to limit their effect on the permeability parameters. Since the stiffness and permeability terms are multiplied together in equation 1 relating the displacement diffusion with the rate of displacement, it would seem sensible that the two sets of parameters would interact with each other affecting the parameterisation of the best fit. Simplistically, halving stiffness would double permeability etc. However only a four dimensional sensitivity analysis (k_0, M, H_{A0} and β) would be able to extract this information, which is beyond the scope of the current paper.

This paper has highlighted some issues with the inverse determination of permeability parameters of cartilaginous tissues from experimental data and the nonlinear biphasic equation. The other alternative is the direct measurement of permeability using a permeation chamber (Mansour and Mow, 1976; Gu et al, 1999; Heneghan and Riches, 2008b). However, due to the compliance of these tissues, an applied fluid pressure across a tissue sample would impart significant strain on the tissue. Thus the zero-strain permeability of the tissue is very difficult to determine using direct methods (Heneghan and Riches, 2008b). Consequently, whilst direct permeation tests are important for the construction of the constitutive equation linking permeability with matrix strain, parameter determination may be best using indirect methods.

Conclusion

Manifolds describing the goodness of fit of the nonlinear biphasic equation to confined compression data suggest that many combinations of parameters that describe permeability yield similar fits. Furthermore, the manifold surface may contain multiple local maxima, associated with surface roughness of the manifold, however, in the cases considered here, the Nelder-Mead simplex method was able to focus on the global maximum, and not converge to a local maximum. Different sampling strategies obtained different permeability parameters, and it has been argued that focussing the data collection on the time-dependent data will provide a more appropriate parameterisation that linear sampling strategies. However, the nonlinear sampling strategy creates the greatest uncertainty in the optimum parameters. It is therefore concluded that such inverse methods, together with any sensible sampling strategy, provide the current best way to determine these parameters but the values determined should be thought of as having large confidence intervals associated with them.

References

Biot MA. 1941. General theory of three-dimensional consolidation. J Appl Phys. 12: 155–165.

Biot MA. 1956. General solutions of the equations of elasticity and consolidation for a porous material. J Appl Mech T-ASME. 23: 91–96.

Ferguson SJ, Keita I, Nolte L-P. 2004. Fluid flow and convective transport of solutes within the intervertebral disc, J Biomech. 37(2): 213–221.

Heneghan P, Riches PE. 2008a. The strain-dependent osmotic pressure and stiffness of the bovine nucleus pulposus apportioned into ionic and non-ionic contributors, J Biomech. 41(11): 2411-2416.

Heneghan P, Riches PE. 2008b. Determination of the strain dependent hydraulic permeability of the compressed bovine nucleus pulposus. J Biomech. 41(4): 903–906.

Holmes MH. 1986. Finite deformation of soft tissue: analysis of a mixture model in uni-axial compression. J Biomech Eng. 108(4): 372-381.

Holmes MH, Mow VC. 1990. The nonlinear characteristics of soft gels and hydrated connective tissues in ultrafiltration. J Biomech. 23(11): 1145-1156.

Guo L-X, Wang Z-W, Zhang Y-M, Lee K-K, Teo E-C, Li H, Wen B-C. 2009. Material Property Sensitivity Analysis on Resonant Frequency Characteristics of the Human Spine. J Appl Biomech. 25(1): 64-72.

Johannessen W, Elliott DM. 2005. Effects of degeneration on the biphasic material properties of human nucleus pulposus in confined compression. Spine. 30(24): E724–E729.

Jones AC Wilcox RK. 2008. Finite element analysis of the spine: towards a framework of verification, validation and sensitivity analysis. Med Eng Phys. 30(10): 1287-1304.

Lai WM, Mow VC. 1980. Drag-induced compression of articular cartilage during a permeation experiment. Biorheology. 17(1-2): 111–123.

Lide DR (Ed.) 1991 CRC Handbook of Chemistry & Physics, 72nd Ed. CRC Press, Boca Raton.

Malandrino A, Planell JA, Lacroix D. 2009. Statistical factorial analysis on the poroelastic material properties sensitivity of the lumbar intervertebral disc under compression, flexion and axial rotation, J Biomech. 42(16): 2780-2788.

Martinez J, Oloyede A, Broom ND. 1997. Biomechanics of load-bearing of the intervertebral disc: an experimental and finite element model. Med Eng Phys 19(2): 145-156.

Mow VC, Kuei SC, Lai WM, Armstrong CG. 1980. Biphasic creep and stress relaxation of articular cartilage in compression: Theory and experiments. J Biomech Eng T ASME 102(1): 73–84.

Périé D, Korda D, Iatridis JC. 2005. Confined compression experiments on bovine nucleus pulposus and annulus fibrosus: sensitivity of the experiment in the determination of compressive modulus and hydraulic permeability. J Biomech. 38(11): 2164–2171.

Rao AA, Dumas GA. 1991. Influence of material properties on the mechanical behaviour of the L5-S1 intervertebral disk in compression – a nonlinear finite element study. J Biomed Eng. 13(2): 139-151.

Riches PE (2010) Indirectly determining permeability: effect of experimental sampling and hold time. Paper presented at CMBBE 2010. Proceedings of the 9th International symposium on Computer Methods in Biomechanics and Biomedical Engineering; 24-27 February; Valencia, Spain.

Riches PE, Dhillon N, Lotz J, Woods AW, McNally DS. 2002. The internal mechanics of the intervertebral disc under cyclic loading. J Biomech. 35(9): 1263-1271.

Soltz MA, Ateshian GA. 2000. Interstitial fluid pressurization during confined compression cyclical loading of articular cartilage. Ann Biomed Eng. 28(2): 150–159.

Tables

Sampling	NM k_0 x10^{-15} m^4/Ns	Map k_0 x10^{-15} m^4/Ns	NM *M*	Map *M*	NM R^2	Map R^2
Nonlinear	12.3 ± 4.91	12.2 ± 4.90	6.86 ± 0.29	6.86 ± 0.30	0.995 ± 0.001	0.995 ± 0.001
0.1 Hz	11.5 ± 5.35	11.4 ± 5.36	6.34 ± 0.34	6.34 ± 0.34	0.962 ± 0.008	0.962 ± 0.008
0.5 Hz	9.68 ± 4.47	9.63 ± 4.42	5.64 ± 0.38	5.64 ± 0.39	0.971 ± 0.006	0.971 ± 0.006
1 Hz	9.63 ± 4.41	9.64 ± 4.41	5.64 ± 0.38	5.64 ± 0.39	0.972 ± 0.006	0.972 ± 0.006

Sampling	Δ k_0 x10^{-15} m^4/Ns	95% Range k_0 x10^{-15} m^4/Ns	Δ *M*	95% Range *M*	Δ R^2	Area (# pixels)	# local maxima
Nonlinear	0.109 ± 0.027	31.5 ± 11.0	0.057 ± 0.017	8.63 ± 0.568	2.37 x 10^{-5}	2103 ± 755	38.8 ± 5.19
0.1 Hz	0.092 ± 0.016	22.1 ± 10.2	0.050 ± 0.013	6.30 ± 0.499	7.89 x 10^{-5}	1701 ± 709	13.8 ± 5.63
0.5 Hz	0.093 ± 0.046	13.9 ± 5.19	0.038 ± 0.006	6.13 ± 0.518	4.25 x 10^{-5}	1417 ± 524	5.38 ± 2.53
1 Hz	0.040 ± 0.007	14.0 ± 5.27	0.045 ± 0.014	6.11 ± 0.501	6.06 x 10^{-5}	1432 ± 540	6.25 ± 2.89

Table titles

Table 1: Permeability parameters for R^2_{max} (mean ± standard error) for the two curve-fitting schemes and for each sampling strategy. NM = Nelder Mead methodology, Map = Mapping methodology.

Table 2: Differences in parameters for R^2_{max} between the two schemes, their range to cover the 95% R^2_{max} area, the area of the region ≥ 95% R^2_{max} and the number of local maxima within that range for each sampling strategy (mean ± standard error).

Figure titles

Figure 1: Diagram of local maximum determination; if the R^2 value using the parameters in the shaded box was greater than all 8 of its immediate neighbours and greater than or equal to $0.95R^2_{max}$, then a local maximum was declared.

Figure 2: Bar chart displaying the average number of sampling frequencies, expressed as a percentage within each epoch, for the nonlinear sampling strategy according to time during the stress relaxation phase.

Figure 3: Solution manifold for sample #5 for the nonlinear sampling strategy. Shading represents R^2 values, and isolines are provided at the 0.9, 0.95 and 0.99 levels. The black thick line describes the travel of the best vertex of the simplex in the Nelder Mead scheme from the original (white) simplex.

Figure 4: Solution manifold for sample #5 for the 0.1 Hz sampling strategy. Shading represents R^2 values, and contours are provided at the 0.9, 0.95 and 0.99 levels. The black thick line describes the travel of the best vertex of the simplex in the Nelder Mead scheme from the original (white) simplex.

Figure 5: Solution manifold for sample #5 for the 0.5 Hz sampling strategy. Shading represents R^2 values, and contours are provided at the 0.9, 0.95 and 0.99 levels. The black thick line describes the travel of the best vertex of the simplex in the Nelder Mead scheme from the original (white) simplex.

Figure 6: Solution manifold for sample #5 for the 1 Hz sampling strategy. Shading represents R^2 values, and contours are provided at the 0.9, 0.95 and 0.99 levels. The black thick line describes the travel of the best vertex of the simplex in the Nelder Mead scheme from the original (white) simplex.

Figure 7a: Typical stress response of a sample over the whole testing period. Dotted line indicates the experimental nonlinear data, whilst the solid lines show the model fits depending on the sampling methodology.

Figure 7b: Depiction of the same stress response as in Figure 7a, but only in the first two minutes of the hold phase. Dotted line indicates the experimental nonlinear data, whilst the solid lines show the model fits depending on the sampling methodology.

$k_{0,i-1}\ ,\ M_{j+1}$	$k_{0,i}\ ,\ M_{j+1}$	$k_{0,i+1}\ ,\ M_{j+1}$
$k_{0,i-1}\ ,\ M_{j}$	$k_{0,i}\ ,\ M_{j}$	$k_{0,i+1}\ ,\ M_{j}$
$k_{0,i-1}\ ,\ M_{j-1}$	$k_{0,i}\ ,\ M_{j-1}$	$k_{0,i+1}\ ,\ M_{j-1}$

Figure 1: Diagram of local maximum determination; if the R^2 value using the parameters in the shaded box was greater than all 8 of its immediate neighbours and greater than or equal to $0.95R^2_{max}$, then a local maximum was declared.
289x91mm (96 x 96 DPI)

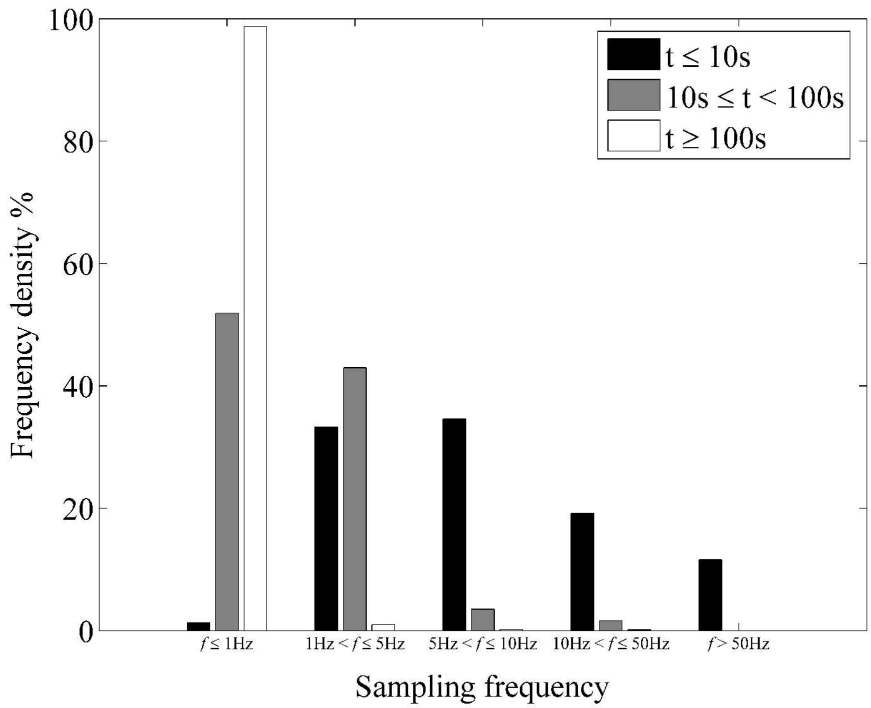

Figure 2: Bar chart displaying the average number of sampling frequencies, expressed as a percentage within each epoch, for the nonlinear sampling strategy according to time during the stress relaxation phase.
203x152mm (600 x 600 DPI)

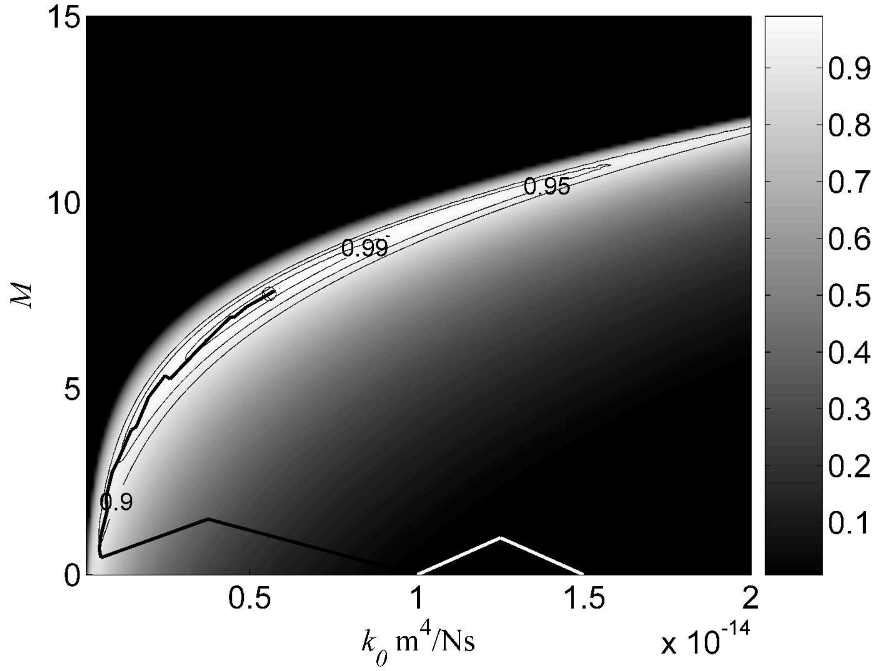

Figure 3: Solution manifold for sample #5 for the nonlinear sampling strategy. Shading represents R^2 values, and isolines are provided at the 0.9, 0.95 and 0.99 levels. The black thick line describes the travel of the best vertex of the simplex in the Nelder Mead scheme from the original (white) simplex.
203x152mm (600 x 600 DPI)

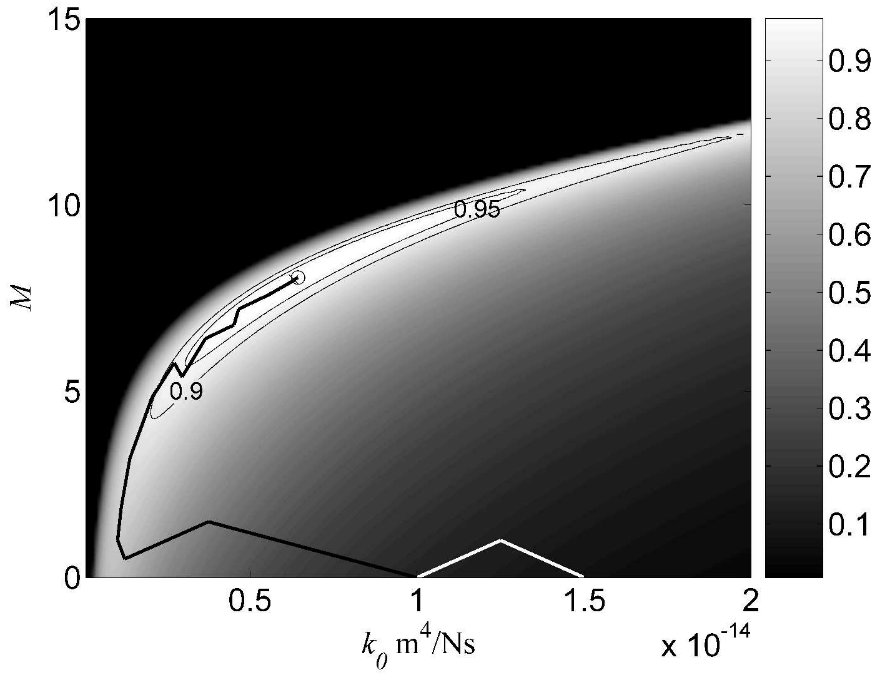

Figure 4: Solution manifold for sample #5 for the 0.1 Hz sampling strategy. Shading represents R^2 values, and contours are provided at the 0.9, 0.95 and 0.99 levels. The black thick line describes the travel of the best vertex of the simplex in the Nelder Mead scheme from the original (white) simplex.
203x152mm (600 x 600 DPI)

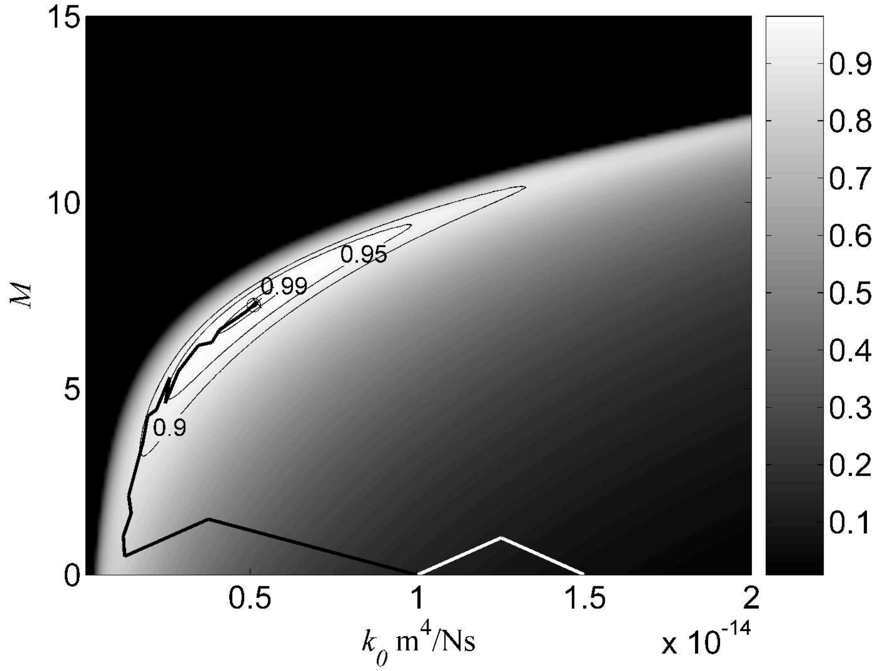

Figure 5: Solution manifold for sample #5 for the 0.5 Hz sampling strategy. Shading represents R^2 values, and contours are provided at the 0.9, 0.95 and 0.99 levels. The black thick line describes the travel of the best vertex of the simplex in the Nelder Mead scheme from the original (white) simplex.
203x152mm (600 x 600 DPI)

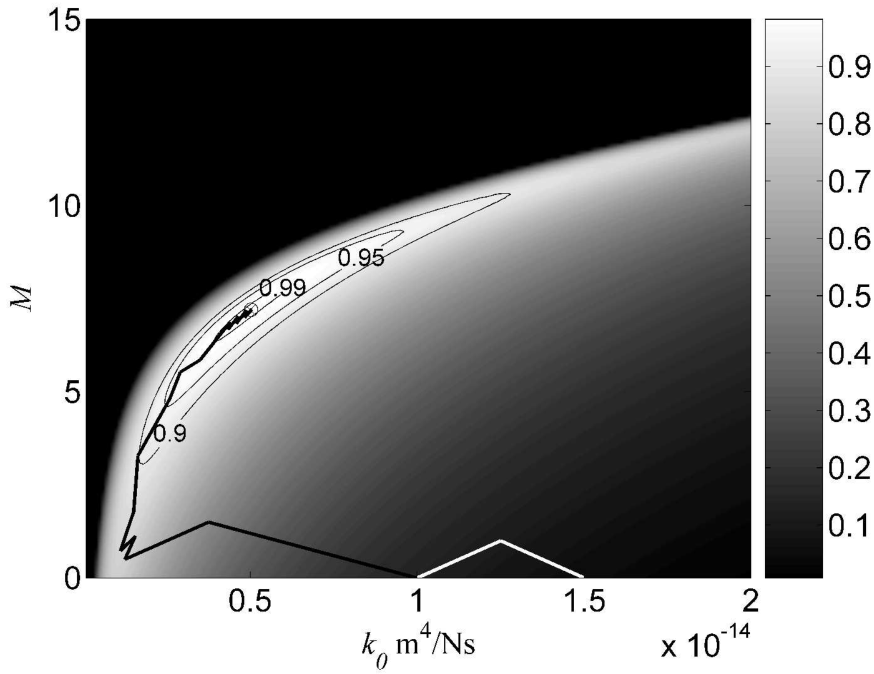

Figure 6: Solution manifold for sample #5 for the 1 Hz sampling strategy. Shading represents R^2 values, and contours are provided at the 0.9, 0.95 and 0.99 levels. The black thick line describes the travel of the best vertex of the simplex in the Nelder Mead scheme from the original (white) simplex.
203x152mm (600 x 600 DPI)

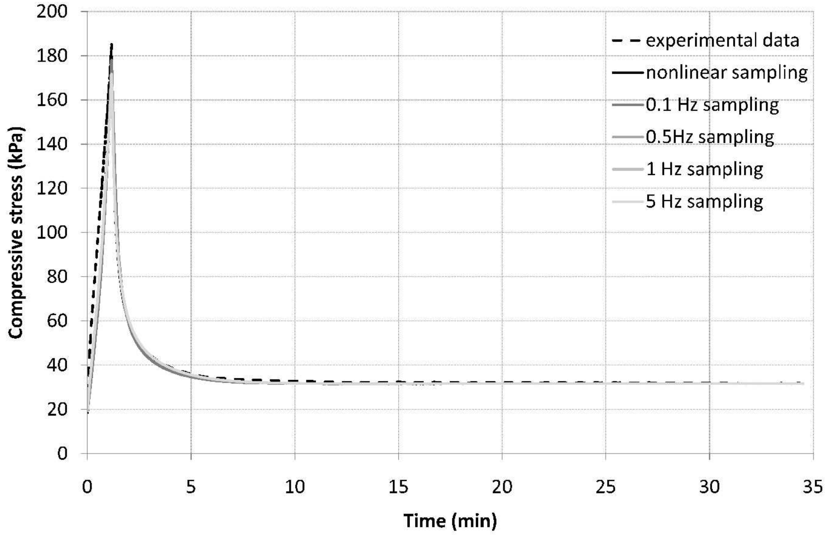

Figure 7a: Typical stress response of a sample over the whole testing period. Dotted line indicates the experimental nonlinear data, whilst the solid lines show the model fits depending on the sampling methodology.
279x215mm (600 x 600 DPI)

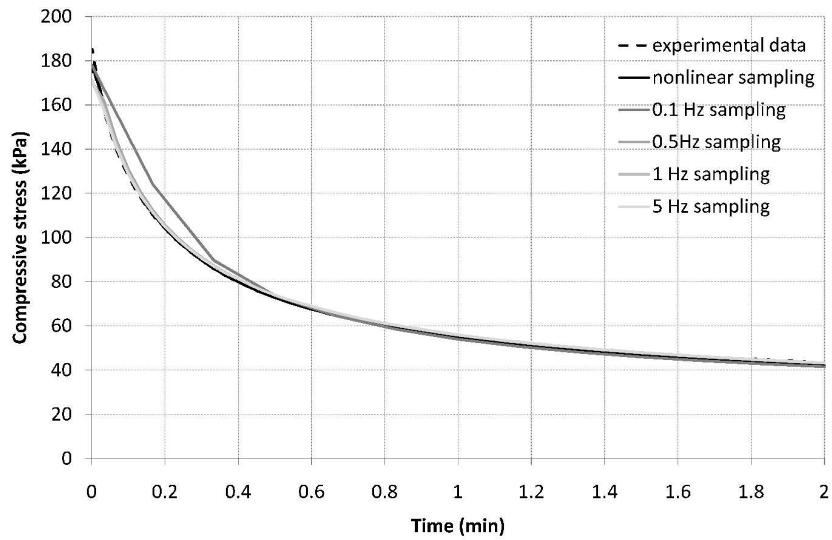

Figure 7b: Depiction of the same stress response as in Figure 7a, but only in the first two minutes of the hold phase. Dotted line indicates the experimental nonlinear data, whilst the solid lines show the model fits depending on the sampling methodology.
279x215mm (600 x 600 DPI)